Connectivity gradients in spontaneous brain activity at multiple frequency bands

Zhu-Qing Gong[1,2], Xi-Nian Zuo[1,2,3,4,*]

[1]State Key Laboratory of Cognitive Neuroscience and Learning, Beijing Normal University, Beijing 100875, China,
[2]Developmental Population Neuroscience Center, IDG/McGovern Institute for Brain Research, Beijing Normal University, Beijing 100875, China,
[3]National Basic Science Data Center, Beijing 100190, China,
[4]Institute of Psychology, Chinese Academy of Sciences, Beijing 100101, China

*Corresponding author: State Key Laboratory of Cognitive Neuroscience and Learning, Beijing Normal University, Beijing 100875, China.
Email: xinian.zuo@bnu.edu.cn, zuoxn@psych.ac.cn

The intrinsic organizational structure of the brain is reflected in spontaneous brain oscillations. Its functional integration and segregation hierarchy have been discovered in space by leveraging gradient approaches to low-frequency functional connectivity. This hierarchy of brain oscillations has not yet been fully understood, since previous studies have mainly concentrated on the brain oscillations from a single limited frequency range ($\sim$ 0.01–0.1 Hz). In this work, we extended the frequency range and performed gradient analysis across multiple frequency bands of fast resting-state fMRI signals from the Human Connectome Project and condensed a frequency-rank cortical map of the highest gradient. We found that the coarse skeletons of the functional organization hierarchy are generalizable across the multiple frequency bands. Beyond that, the highest integration levels of connectivity vary in the frequency domain across different large-scale brain networks. These findings are replicated in another independent dataset and demonstrated that different brain networks can integrate information at varying rates, indicating the significance of examining the intrinsic architecture of spontaneous brain activity from the perspective of multiple frequency bands.

Key words: spontaneous oscillations; frequency; gradient; fMRI; connectivity.

Introduction

The intrinsic functional architecture of the brain is reflected in spontaneous brain oscillations as measured by resting-state functional magnetic resonance imaging (rs-fMRI). From spontaneous brain activity, several large-scale brain networks dominant in different functions have been discovered (Yeo et al. 2011). This indicates that even in the absence of tasks, brain areas that are dominant in the same functions display comparable connectivity patterns. In contrast to network or parcellation analysis, which stresses the universality within networks and the heterogeneity among networks or parcels, gradient analysis based on functional connectivity (FC) features demonstrates continuous similarity changes across the cortex (Huntenburg et al. 2018). The FC matrix could be rearranged into a collection of gradients by using dimension reduction procedures. Each gradient is represented by a one-dimensional axis. The position of a particular brain region on the gradient axis reflects the degree of function in the function scale that it represents. The first two gradients are thought to reflect relatively straightforward physiological significance (Margulies et al. 2016). The first gradient, or the principal gradient, accounts for the majority of variance in the FC matrix. On one end of the first gradient axis are unimodal primary areas, and on the other end are high-level transmodal associative areas. The first gradient spreads brain areas of different processing levels on a continuous axis and reflects how information is processed hierarchically in the spatial domain from primary sensorimotor regions all the way up to the associative regions. As a corollary, it captures the cortical functional integration feature. And a particular brain region's position on this axis reflects its degree of functional integration across the entire cortex. Besides, the distribution of the first gradient is consistent with the gradient change in gene expression as well as cortical microstructure (Hawrylycz et al. 2012; Huntenburg et al. 2017). This indicates that the hierarchical organization of the spontaneous brain oscillations reflects the brain's intrinsic architecture. The second gradient depicts functional segregation among the primary unimodal regions. The gradient axis serves to partition different sensorimotor areas. Therefore, both functional integration and functional refinement can be seen in the way that neuronal oscillations are organized when these two gradients are combined.

These results, however, only consider brain oscillations within the traditional resting-state frequency range ($\sim$ 0.01–0.1 Hz); oscillations at higher and lower frequencies are ignored. In other words, studies of gradients in the traditional frequency range only capture the spatial organization of oscillations in a limited spectral range. Higher and lower frequencies, however, should also be taken into account in order to investigate brain activity in a more comprehensive manner, as they also carry valuable neural information (Yan et al. 2009; Zhang et al. 2015; Frühholz et al. 2020). Evidence from research using various measuring techniques has demonstrated that brain oscillations at different frequencies are prevalent in different brain processes and correlate with different psychological states. According to a recent fMRI study, different states of consciousness were associated with frequency-specific power differences in blood oxygen level-dependent (BOLD) signals in the rat brains (Cabral et al. 2023). Early electrophysiological

research has shown that fast oscillations correspond to local activity and primary sensory processing, whereas slow oscillations correspond to remote synchronization and high-order activities (Kopell et al. 2000; Engel et al. 2001; Buzsaki and Draguhn 2004). This frequency feature is supported by the anatomy of neural fibbers (Aboitiz 1992). Local sensorimotor brain areas are mostly connected by thick, highly myelinated fibbers that conduct signals fast. Remote and high-level brain regions are linked by thin, less myelinated fibbers that transport signals at a slower rate. This physiological trait establishes the independence of measurement methods for the frequency-dependent nature of brain signals. Hence, both frequency and spatial domain should be taken into account in fMRI research in order to further decipher the tangled brain processes. Although the majority of rs-fMRI discoveries were made in the traditional resting-state frequency range, an increasing number of fMRI studies using multiband frequency analysis in the last decade have found that the characteristics of BOLD oscillations are also frequency-dependent (Zuo et al. 2010; Baria et al. 2011; Xue et al. 2014; Li et al. 2018; Li et al. 2021). Similar to electrophysiological evidence, BOLD oscillations in low frequency bands have more long-distance connections than in high-frequency bands; additionally, low frequency brain networks contribute more to global efficiency than high-frequency brain networks, which suggests that slow oscillations might predominate more in functional integration and high-level functions (Thompson and Fransson 2015; Jamadar et al. 2018; Park et al. 2019). This suggests that BOLD oscillations in different frequency bands have different spatial arrangements and functions. Furthermore, these discrepancies may also be seen in the connectivity gradient patterns across frequency bands. Therefore, the organization architecture of spontaneous brain activity should be examined in the full detectable frequency range rather than just focusing on one narrow spectra (e.g. the traditional rs-fMRI frequency range). When combining the spatial, temporal, and frequency dimensions, it may be possible to determine the processing speed of different brain areas as well as potential information transmission pathways.

The intrinsic organization hierarchy of BOLD oscillations in the full detectable frequency range has very seldomly been studied to this point. One of the reasons behind this, aside from the lack of awareness of the significance of multiband analysis in fMRI research, is that the signal-to-noise ratio of the early MRI scanners used in research was insufficient to identify neural signals in frequencies outside the traditional rs-fMRI frequency range. The power spectrum measured was therefore mostly centered between 0.01 and 0.1 Hz (Biswal et al. 1995). Moreover, higher frequencies could not be reached due to the slow sample rates. The finest opportunity to explore this issue has been made possible by the development of magnetic resonance devices with higher sampling rates and stronger signal-to-noise ratios. Almost the whole range of slow oscillations (from slow-1 to slow-6) on the frequency axis defined by the natural logarithm linear law (N3L) can be covered by a sufficiently long fast scan (Penttonen and Buzsáki 2003). According to the classification of N3L, the traditional rs-fMRI frequency range is the summation of slow-4 and slow-5 bands. In the current study, we extended the frequency range to slow-1 to slow-6, and aim to illustrate the intrinsic organization hierarchy of BOLD oscillations in the full detectable frequency range by performing gradient analysis across multiple frequency bands of fast rs-fMRI signals from the Human Connectome Project (HCP). We mainly focused on the first two gradients since they have rather obvious physiological relevance. By depicting the distribution patterns of these two gradients across frequency bands,

we investigated how functional integration and segregation are arranged across the cortex in the frequency domain. We also identified the frequency band at which certain brain regions exhibit the highest integration level based on the frequency-rank of the greatest values of the first gradient. By doing so, a brain map that reflects the highest integration rate of the cortex could be generated. We anticipated that brain regions that differ in the integration level in the spatial domain would also differ in the frequency domain.

Materials and methods
Data acquisition and preprocessing

Resting-state fMRI data with a high sampling rate and extended scan duration from the HCP-339 unrelated datasets were chosen for this research to acquire a wider frequency range (Van Essen et al. 2013). The resting-state data were collected in the adjacent two days. Two runs of resting-state sequence were scanned each day. The first run was coded from left to right, and the second run was from right to left. The length of each run was 14 minutes, 33 seconds. The scanning parameters were as follows: sequence = gradient-echo EPI; TR = 720 ms; TE = 33.1 ms; flip angle = 52; FOV = 208 mm × 180 mm; matrix = 104 × 90; slice thickness = 2 mm (72 slices; 2 mm isotropic voxels); multiband factor = 8; echo spacing = 0.58 ms; bandwidth = 2,290 Hz/Px; volumes = 1,200. The HCP dataset is described in depth in (Van Essen et al. 2013). The data were preprocessed according to the HCP minimal preprocessing pipeline with the ICA-FIX denoising procedure (Glasser et al. 2013). The preprocessing procedures included (i) gradient distortion correction; (ii) motion correction; (iii) EPI image distortion correction; (iv) registration to the T1w image; (v) one-step spline resampling; (vi) intensity normalization and brain masking; (vii) transfer volume-based time series into surface-based time series; and (vii) ICA-FIX denoising. The preprocessed time series were then decomposed into six frequency bands (slow-6: 0.007–0.012 Hz; slow-5: 0.012–0.030 Hz; slow-4: 0.030–0.082 Hz; slow-3: 0.082–0.223 Hz; slow-2: 0.223–0.607 Hz; slow-1: 0.607–0.694 Hz) using DREAM (Gong et al. 2021).

Gradient analysis

First, four FC matrices (64,984 × 64,984) in each band were produced by performing a whole-brain vertex-based FC analysis on each run for all frequency bands at the individual level. The four matrices were then averaged in each band after each FC matrix underwent the Fisher-Z transform. One FC matrix was created in this manner for each participant in each band. The group-level FC matrix was then calculated for each frequency band by averaging all the individual-level FC matrices in the same band. Next, we performed gradient analysis on each group level matrix using the *Brainspace* toolkit (Wael et al. 2020). The matrix was first made sparse by preserving the top 10% values for each vertex and setting the remaining values to 0. Then, using the cosine similarity approach, an affinity matrix (64,984 × 64,984) was produced by computing the FC similarity between each pair of vertices. The affinity matrix's dimension was then reduced using diffusion map embedding, which also divided the matrix into a few eigenvectors. The gradient values of all brain areas are contained in each eigenvector.

Frequency-rank analysis

After gradient analysis, we obtained six first gradient vectors, one for each frequency band. When the directions of these vectors are aligned, and the gradient values are normalized in each vector, the

position across vectors would be comparable. Since the first gradient reflects the transition of connectivity pattern from unimodal via multimodal to transmodal regions, the relative position of a vertex along the first gradient can indicate whether the function of the vertex is more basic and unitary (e.g. more toward the unimodal end) or more advanced and integrated (e.g. more toward the transmodal end). A vertex's position along the first gradient can therefore, from the angle of frequency dimension, reflects in which frequency band its function is more unitary and in which is more integrated. Based on this, we performed the frequency-rank analysis to identify the frequency band in which each vertex has the highest level of integration. We started by lining up the orientation of the six vectors. Each vector was then transformed into z-scores. The z-scores were then sorted across six frequency bands for each vertex, and the sorted values were assigned to the corresponding frequency bands. Finally, according to the ranking data, we extracted two maps, one depicting the frequency band with the highest gradient value and the other representing the frequency band with the lowest gradient value. The high-value frequency-rank map could reflect the frequency bands at which brain regions show the highest level of integration. The frequency information contained in the map can further reflect the rate at which the cortex performs its highest integration function. As a supplement, we performed frequency-rank analysis for the second gradient as well.

The global Moran test

To testify whether the spatial pattern of the high-value frequency-rank map is spatially clustered or randomly distributed, we performed the global Moran test. We first calculated Moran's I, an index measures spatial autocorrelation, which refers to the correlation between adjacent positions of signals in space (Moran 1948). Because the index is multi-dimensional and multi-directional, it can reflect the global spatial information better than one-dimensional correlation. Moran's I is computed according to formular (1):

$$I = \frac{N\sum_{i=1}^{N}\sum_{j=1}^{N}w_{ij}\left(x_i - \overline{x}\right)\left(x_j - \overline{x}\right)}{W\sum_{i=1}^{N}\left(x_i - \overline{x}\right)^2} \quad (1)$$

where N is the number of vertices indexed by i and j; x is the variable of interest; w_{ij} is the spatial weight matrix that reflects the weight of the distance between every two positions; and W is the sum of all w_{ij}. The null hypothesis of the global Moran test is that the spatial pattern of variables is randomly distributed. A positive Moran's I with a statistically significant P-value indicates the spatial pattern is spatially clustered, whereas a negative one indicates a spatially dispersed pattern. If the P-value is not statistically significant, then the null hypothesis cannot be rejected. The statistical significance of the spatial distribution can be obtained by calculating the Z-score of the Moran's I:

$$z_i = \frac{I - E[I]}{\sqrt{V[I]}} \quad (2)$$

where $E[I]$ is the expectation value of I and $V[I]$ is the variance of I, which are computed as follows:

$$E[I] = -\frac{1}{n-1} \quad (3)$$

$$V[I] = E[I^2] - E[I]^2 \quad (4)$$

Meta-analytic decoding of the high-value frequency-rank map

We used the *NeuroSynth* meta-analytic database (www.neurosynth.org) to evaluate the functional terms associated with the brain regions showing the highest first gradient values in each frequency band in order to further validate the neurocognitive meaning of the high-value frequency-rank map of the first gradient. The first step was to construct and project a surface mask for each frequency band into the MNI152 standard space. The similarity between each mask and the complete collection of 1,307 *NeuroSynth* terms was then determined. All terms were listed in descending order by correlation coefficients. Terms related to brain anatomy were then removed (e.g. prefrontal), and the top five terms with cognitive implications for each frequency band were chosen. If within the top five terms there were more than one terms referring to the exact same function (e.g. pain and painful), we only kept the first one.

Reproducibility analysis

In recent years, more and more, researchers have pointed out that the reproducibility crisis in the field of fMRI has been largely overlooked (Noble et al. 2019; Zuo et al. 2019; Marek et al. 2022). Although the reliability of FC gradient derived with a scan of duration less than 20 minutes is below moderate (Hong et al. 2020; Zhang and Zang 2023), the gradient distribution pattern in the traditional frequency range has been reproduced at the group level across different studies (Margulies et al. 2016; Nenning et al. 2023; Samara et al. 2023). This shows that the gradient analysis is a reliable method at group level. However, the multi-band gradient distribution pattern has not been studied yet, let alone reproduced. To testify the reproducibility of the multi-band results, we performed the same frequency analysis and the frequency-rank analysis based on the Chinese Human Connectome Project (CHCP) dataset. It is the counterpart of the HCP that utilized a comparable protocol for the data collection. Details of subject information, data parameters, and preprocessing procedure can be found in Ge et al. (2023). It should be noted that the CHCP BOLD oscillations could be decomposed into only five frequency bands (slow-1 to slow-5) because the CHCP resting-state scan duration is shorter than the HCP resting-state scan duration. We thus performed the frequency-rank analysis on these five frequency bands of the HCP data to make sure the frequency-rank maps are comparable between the two datasets.

Results
The proportion of variance explained by gradients

Gradient analysis produced a set of gradient vectors for each frequency band. The gradient vectors are arranged according to the amount of FC matrix variance they can explain. For instance, the first gradient explains the most variance. Slow-3 to slow-6 demonstrate the same tendency, as shown in Fig. 1. Beginning about the 50th gradient, the explanation of variance tends to be zero, with the front gradients explaining far more variance than the back gradients. Slow-1 and slow-2 exhibit a similar tendency, but the amount of variance explained by each gradient differ.

Gradient distribution across frequency bands

We primarily concentrated on the distribution patterns of the first two gradients across frequency bands because they account for the majority of variance in the FC matrix and have relatively
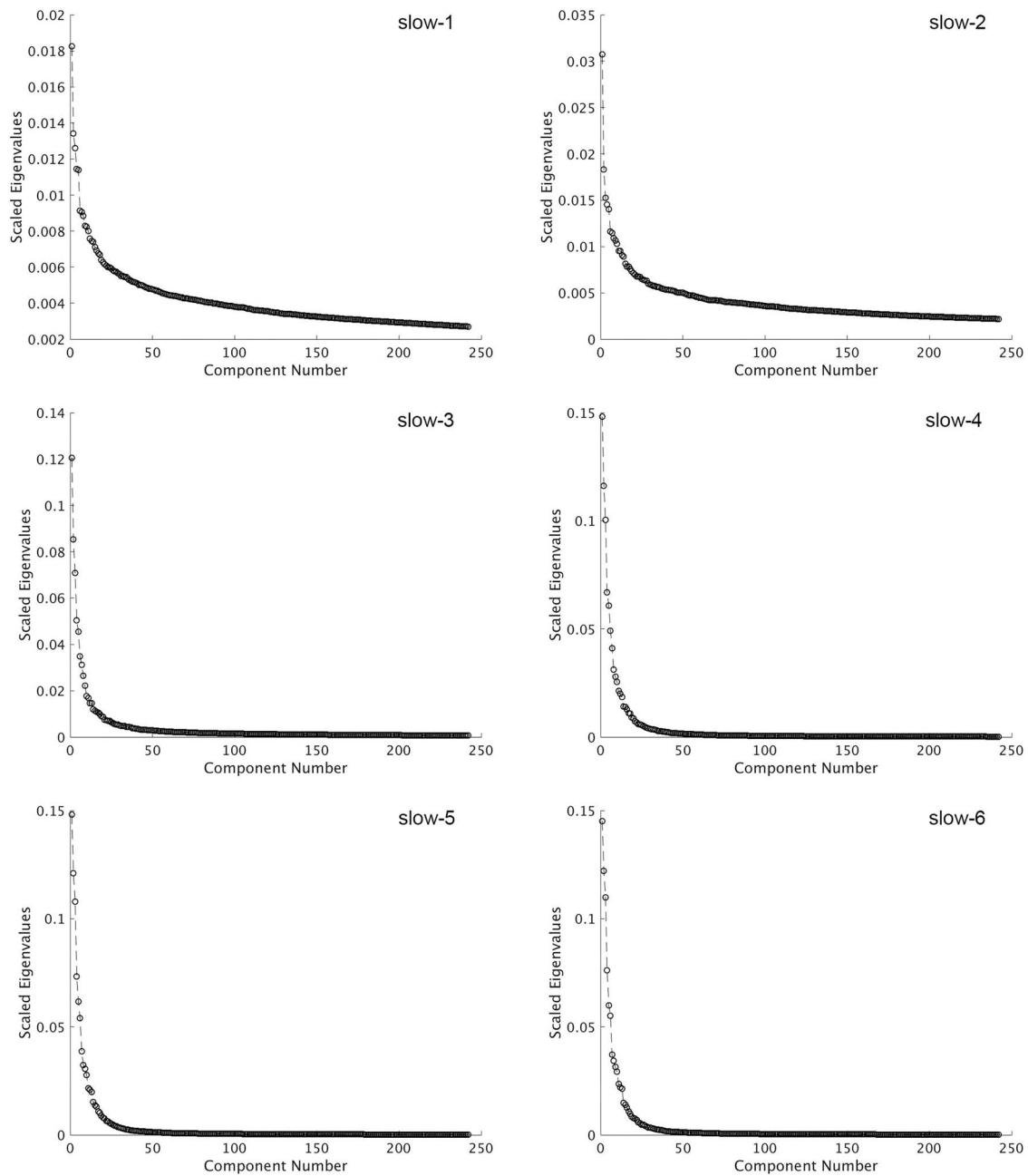
Fig. 1. The variance explained by each gradient across six frequency bands. Each point in the diagram represents a gradient component. The vertical axis represents the proportion of variance that each gradient component can explained. The tendencies are similar across frequency bands, but the amount of variance explained by each gradient differs less in slow-1 and slow-2 from that in lower frequency bands.

obvious physiological implications. The distribution patterns of the first two gradients from slow-1 to slow-6 are shown in Fig. 2. The general distribution patterns of the first gradient are comparable throughout all six bands, whereas slow-1/2 and the lower frequency bands differ in some specifics. In all frequency bands, the first gradient clearly shifts from unimodal to transmodal regions. However, the unimodal end of the first gradient anchors in sensorimotor regions in slow-3 to slow-6, whereas in slow-1, it anchors in the visual cortex. Slow-2 shows a transition mode from slow-1 to lower bands, of which the unimodal end anchors in both sensorimotor and visual cortex. This characteristic is more clearly shown in Fig. 3. The color of the scatter plots indicates the position of each vertex on the cortex. In slow-3 to slow-6, the unimodal end of the first gradient, or the points in the

scatter plot at the minimum of the first gradient axis, is represented by purple, which distributed in the motor cortex. In slow-1 and slow-2, the unimodal end points are dark blue, which distributed in the visual cortex in slow-1 and both visual and sensorimotor cortex in slow-2. In addition, the transmodal end of the first gradient is more focalized in the lateral part of the transmodal regions in slow-1/2 compared with lower frequency bands.

The general distribution pattern of the second gradient is consistent in slow-3 to slow-6, which shows the segregation among the primary sensorimotor regions. It should be noted that slow-1 and slow-2 show different patterns. Extreme values in a restricted region of the anterior medial temporal lobe interfere with the visualization of the second gradient in slow-1 (see Fig. 2B).
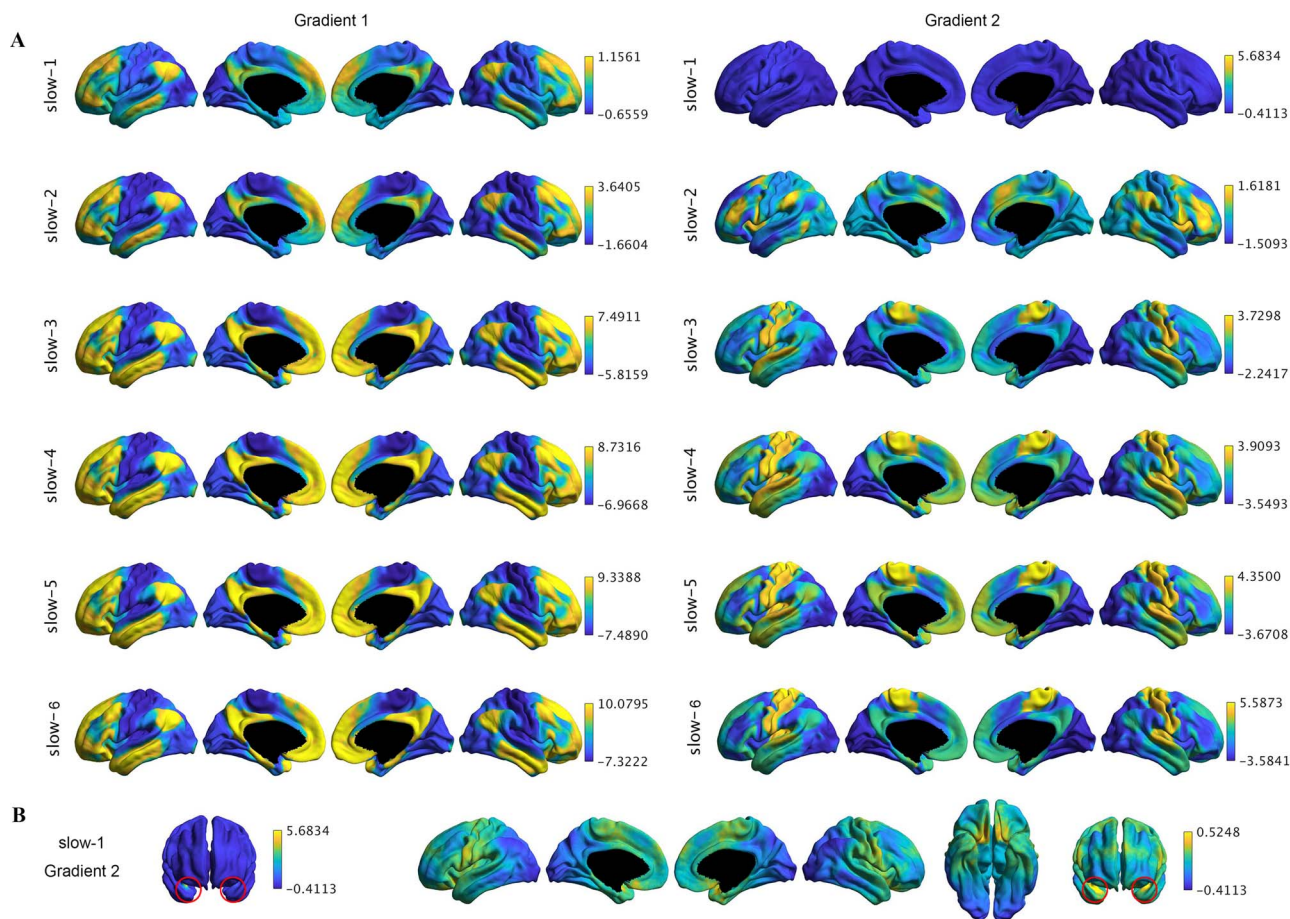
Fig. 2. The distribution of the first and second gradient across six frequency bands. (A) The general distribution patterns are comparable throughout all six bands, whereas slow-1/2 and the lower frequency bands differ in some specifics. (B) Extreme values in a few localized areas of the anterior medial temporal cortex interfere with the visualization of the second gradient of slow-1. After thresholding, we can see that the gradient distribution of slow-1 also goes from the visual cortex to the auditory cortex and finally reaches the sensorimotor cortex.

After thresholding, we can see that the gradient distribution of slow-1 also goes from the visual cortex to the auditory cortex and finally reaches the sensorimotor cortex. The gradient change, however, is not as noticeable as it is in lower frequency bands. A different gradient pattern can be seen in slow-2, where the task-positive regions are located on one end of the axis and parts of the DMN are located on the other. Furthermore, this gradient pattern resembles the third gradient in the slow-3 to slow-6 bands. The extreme values in slow-1 suggest that gradients at high frequencies may be noise-sensitive. Since the amounts of variation explained by each gradient in slow-1 and slow-2 are quite close, we speculate that the order of gradients in slow-1/2 may likewise be noise- and preprocess-sensitive.

Results of frequency-rank analysis and the global Moran test

The frequency-rank maps for the two gradients are shown in Fig. 4. The frequency-rank map of the highest values for the first gradient represents the frequency band where a certain brain region is the most toward the transmodal end, as shown in Fig. 4(A). In slow-1, for example, relative to other frequency bands, a brain region operates the most like transmodal regions or exhibits the highest level of integration if it is the closest to the transmodal end among all six bands. Furthermore, it can be inferred that this brain region performs its highest integration function at a rate in the frequency range of slow-1 because

frequency provides information about speed. Thus, Fig. 4(A) reflects the highest integration rate across the cortex. And in the present work, we primarily focus on discussing this map. The spatial distribution of the highest integration rate apparently exhibits clustered spatial pattern rather than stochastically distributed. It's interesting to note that the contour of the clustered pattern approximately outlines the shapes of the resting-state networks. To testify the significance of the spatially clustered pattern, we performed the global Moran test for each hemisphere. Both hemispheres show significant spatially clustered patterns (left hemisphere: $I = 0.1134$, $z = 620.2489$, $P = 0.0000$; right hemisphere: $I = 0.1045$, $z = 591.0687$, $P = 0.0000$). In general, the primary sensory and motor networks mainly show the highest integration level in high-frequency bands (except for part of the visual network), while high-level networks exhibit divergent patterns. Specifically, the DMN is divided into two regions. The medial region of the DMN has the highest level of integration in slow-6, whereas the lateral part exhibits the highest level of integration in slow-1. The ventral attention network (VAN) is also partitioned. The lateral and medial parietal lobe VAN areas in slow-5 and slow-6 exhibit the highest levels of integration. Areas in the ventral lateral frontal lobe have the highest level of integration in slow-1 to slow-4. The frequency distributions of the highest integration level of the dorsal attention network (DAN) and the frontoparietal network (FPN) are more inner consistent. The DAN shows the highest integration level in the low frequency
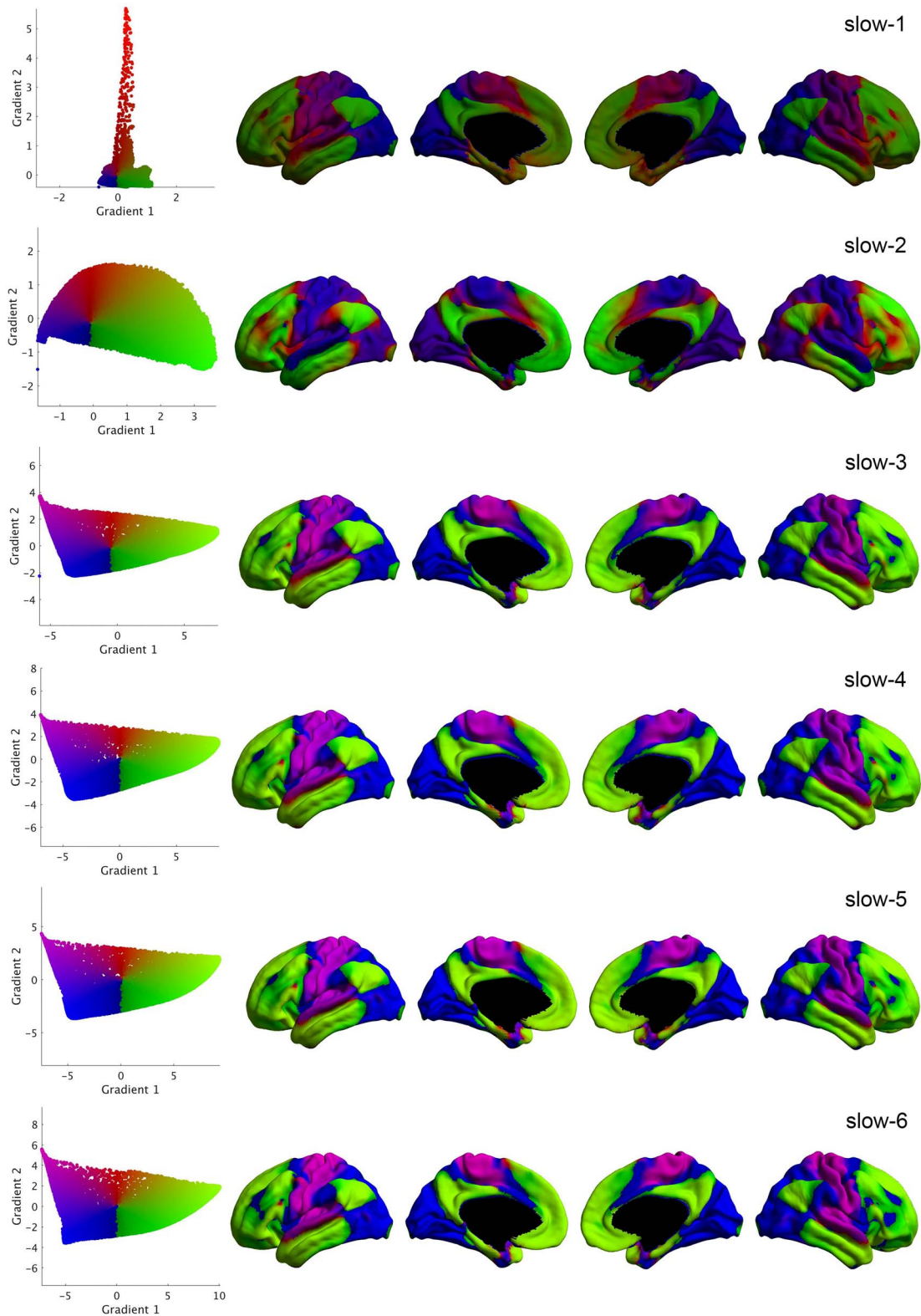
Fig. 3. The Euclidean distribution of the first and second gradient across six frequency bands. The color of the points in the scatter plot indicates the location of these points on the cortex, as depicted on the left. In slow-1 and slow-2, the points at the unimodal end of the first gradient are dark blue. The dark blue points are situated on the visual cortex in slow-1 and both the visual and sensorimotor cortex in slow-2, as indicated on the left cortical maps. In slow-3 to slow-6, the unimodal end points are purple, which are all located on the sensorimotor cortex.
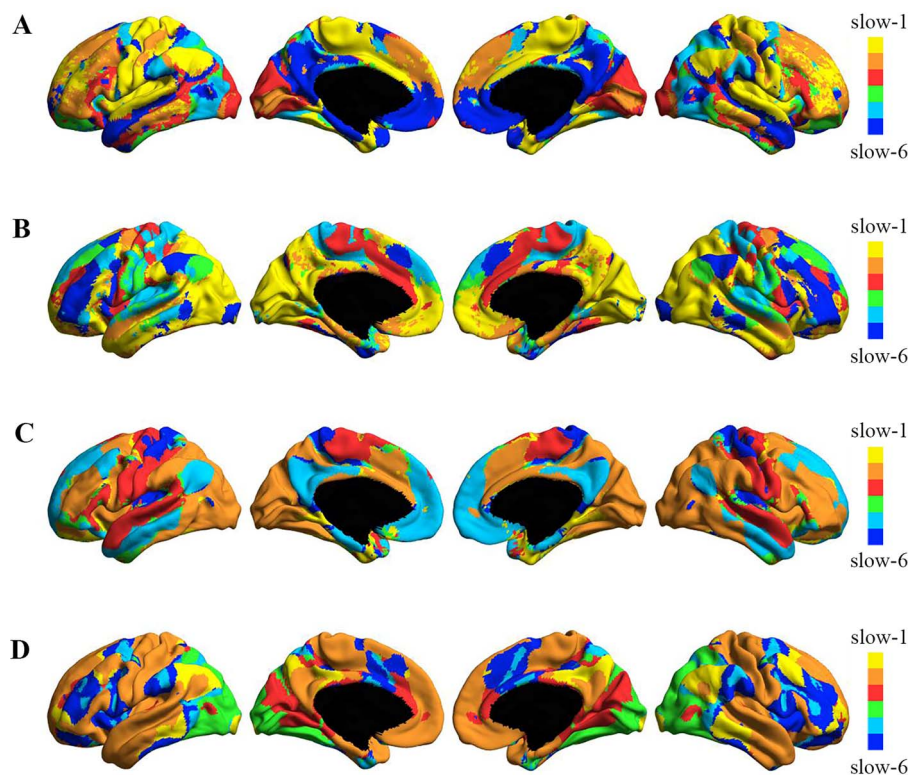
Fig. 4. The frequency-rank map of the first two gradients. (A) The frequency-rank map of the highest values for the first gradient reflects the frequency band where a particular brain area has the highest level of integration. (B) The frequency band where the most basic functional level of a particular brain area is present is indicated by the frequency-rank map of the lowest value for the first gradient. The frequency-rank map of the highest and lowest values for the second gradient are shown in (C) and (D), respectively.

bands (slow-5 and slow-6), whereas the FPN in the high-frequency bands (slow-1 and slow-2). The highest level of integration of primary networks is mainly in the high-frequency bands. In slow-1 and slow-2, the auditory network (AN) and the somatomotor network (SMN) show the highest levels of integration. In slow-2/3 and slow-5, the visual network (VN) exhibits the highest levels of integration. The frequency band where the most basic functional level of a particular brain area is present is indicated by the frequency-rank map of the lowest value for the first gradient. Figure 4(B) shows that the distribution pattern is practically the inverse of the high value map. Figure 4(C)–(D) displays the two maps for the second gradient, which illustrate the frequency band at which a particular brain region exhibits the most connectivity similarity to the visual or sensorimotor cortex.

Meta-analytic functions of each frequency band

We conducted a meta-analytic decoding for the high-value frequency-rank map of the first gradient using the *NeuroSynth* database in order to further examine the meaning provided by the frequency-rank map. Table 1 lists the top five functional terms associated with each frequency band's highest-ranking brain regions. The top functional terms in each band, except for slow-2, are rather homogeneous. Slow-1's highest frequency-ranking brain areas are primarily linked to sensory and motor processes. Slow-2's correlation coefficient values are lower than those of other bands and it is related with functional items that are diverse. Slow-3 is mostly associated with language-related functions. Most slow-4 terms have relevance with executive function. Slow-5 is associated with visual, spatial, and attention functions. Slow-6 terms are mostly concerning self-related and social cognitive functions.

Multi-band gradient patterns of the CHCP dataset

The same frequency-rank analysis and gradient analysis were repeated on the CHCP dataset to demonstrate the reproducibility of the multi-band gradient analysis. The multi-band gradient distribution of the CHCP is consistent with the HCP (see Fig. S1). The unimodal-transmodal axis appears as the first gradient in all five frequency bands. The visual-sensorimotor axis appears as the second gradient in all bands except slow-2. Same as the HCP, the slow-2 second gradient of the CHCP displays the transition from the task-positive regions to task-negative regions. Like the HCP results, Fig. S2 shows in slow-1 and slow-2 the unimodal end of the first gradient differs from lower frequency bands. In lower frequency bands, the unimodal end anchors in the sensorimotor cortex, but in slow-1 and slow-2 it anchors in both the visual and sensorimotor cortex. The comparison of frequency-rank maps between the HCP and the CHCP is shown in Fig. S3. The frequency-rank analysis was carried out in slow1-slow5 for the HCP data as well to ensure that the maps are comparable between the two datasets. Although some specifics of the first gradient's highest rank map differ across the two datasets, the overall patterns are identical. The frequency-rank maps of the second gradient show some clear differences across datasets. For example, in the HCP dataset, the DMN is located closest to the sensorimotor cortex on the second gradient axis in slow-5, whereas in the CHCP dataset, it is located closest in higher frequency bands (Fig. S3C). The mechanism behind the differences between the two datasets is worthwhile to further investigate. Since there are just five frequency bands in the replicative frequency-rank analysis, further explanation of the cognitive meaning of these maps is not necessary here. We will focus on discussing the six-band frequency-rank map of the HCP dataset in the following part.

Table 1. Meta-analytic decoding of the frequency-rank map.

	The top five functional terms (correlation coefficient)
slow-1	Somatosensory (0.237), primary motor (0.199), sensorimotor (0.191), pain (0.184), auditory (0.167)
slow-2	Self referential (0.058), primary visual (0.058), executive (0.054), primary somatosensory (0.053), remembering (0.051)
slow-3	Early visual (0.106), lingual (0.104), verb (0.093), visual (0.089), semantic (0.089)
slow-4	Olfactory (0.135), arithmetic (0.094), spatial (0.082), working memory (0.077), calculation (0.075)
slow-5	Visual (0.243), spatial (0.201), spatial attention (0.201), eye (0.200), attention (0.194)
slow-6	Autobiographical (0.217), episodic (0.178), social (0.161), memories (0.153), theory of mind (0.151)

Discussion

In this study, we examined the distribution of the first and second FC gradients over six frequency bands. We found both consistency and differences of gradient patterns across frequency bands. We discovered that the coarse skeleton of the functional organization is stable across frequencies. However, the slow-1/2 and lower frequency bands had differences in some specifics. This indicates that, the large-scale functional organization is consistent across frequencies, which might be driven and constrained by neurophysiological characteristics. Whereas, in some details, the integration and segregation patterns between high and low frequencies are different, which reflects there exists differences in function between high and low frequency oscillations. To further explore the differences across frequency bands, we performed frequency-rank analysis on the gradient maps, and found that different networks can integrate information at varying rates and that subregions of the DMN and the VAN diverged in the frequency domain, whereas other networks were relatively homogeneous.

The coarse skeletons of the functional organization architecture are generalizable across the multiple frequency bands

According to our analysis, in spatial dimension, the distribution patterns of the first two gradients are generally stable across frequency bands. And these spatial patterns are consistent with previous single band studies (Margulies et al. 2016; Dong et al. 2021; Samara et al. 2023). This indicates that the main variance of FC in different frequency bands has the same driving mechanism. A recent study has shown that the sensorimotor-transmodal axis appeared as the principal gradient through the entire range of connectivity levels (Nenning et al. 2023). Our results further demonstrated that this axis emerged as the principal gradient across all frequency bands as well. The prominent position of the sensorimotor-transmodal axis across connection levels and frequency bands suggests that essential traits, such as physiological organization, should be the driving force of the first gradient. As physical connection is the basis of functional connection, the main driving mechanism should be the anatomical pathways and physical attributes of the brain. There is some evidence supporting this view. The intracortical myelin and gene expression of the cortex both show a gradient change along the unimodal-transmodal axis (Huntenburg et al. 2018). In addition, recent studies have revealed the presence of network organization in white matter and the corresponding relationship between white matter networks and resting-state networks (Peer et al. 2017; O'Muncheartaigh and Jbabdi 2018). Further research is needed to determine whether there are corresponding gradient changes among white matter networks. This physiologically based frequency consistency maintains that the functional categories of a given brain region or brain network are constant across frequency bands. In other words, in the spatial axis, the approximate location of a brain region's integration level is essentially constant across frequency bands. For instance, the visual cortex is primarily involved in processing visual information; therefore, its integration level should be lower across frequencies compared with the prefrontal cortex, whose functional level is more abstract. This is true even though the exact function of the visual cortex may vary depending on the frequency.

Although the coarse skeleton of the functional organization is similar across frequencies, the exact location of the unimodal end is different between slow-1/2 and lower frequencies in both datasets. The unimodal end is anchored in the visual cortex in slow-1/2, whereas it is anchored in the sensorimotor cortex in lower frequencies. This suggests that the integration processes of different sensory modules might be different in the frequency domain. We note that, in both datasets, the task-positive to task-negative axis emerged as the second gradient in slow-2. Brain regions at the task-positive end largely overlapped with the FPN and the VAN. And the task-negative end anchored in the DMN. The FPN and the VAN negatively interplay with the DMN both temporally and spatially, and in both resting- and task-state (Chen et al. 2013; Leech et al. 2014). Given that the FPN and a portion of the VAN exhibit the highest integration rates in high-frequency bands on the frequency-rank map, the second gradient in slow-2 may reflect the predominance of stimuli-related cognitive control in slow-2.

Frequency-rank map reflects that brain networks integrate information at varying rates

From a global perspective, the frequency-rank map of the highest value for the first gradient is consistent with the spatial structure of the large-scale brain networks (Yeo et al. 2011), indicating that a common intrinsic large-scale architecture underpins both the spatial and frequency functional organization. The frequency-rank cluster of the primary sensory and motor networks (SMN, AN, and most part of VN) is comparatively homogeneous, with all of them operating at the highest order in high-frequency bands (slow-1 to slow-3). This is in line with previous discoveries that high-frequency bands display the most power in these networks (Gohel and Biswal 2015). However, there are still discrepancies between AN/SMN and VN. The AN in slow-1 exhibits the highest integration level. The SMN performs at the highest order mainly in slow-1, with part of the postcentral gyrus operating in slow-2. Additionally, the meta-analytic decoding results show that slow-1 is mainly associated with somatosensory, motor and auditory functions. This illustrates the integration process of these primary functions is in high-frequency bands. The lowest rankings of these two networks are mainly in the low- and medium-frequency bands (slow-3 to slow-5), implying that the integration direction of these two networks is from low frequency bands up to high-frequency bands. Most part of the VN performs at the

highest integration level in slow-2 and slow-3, whereas a region in the lateral VN is in slow-5. The lowest rankings of the VN are mainly in slow-1, except for the lateral posterior visual cortex that is in slow-6, which suggests there may be two types of visual pathways opposite in direction. One type integrates information from higher frequency (slow-1) to lower frequency (slow-2/3 and slow-5), the other integrates information from lower frequency (slow-5) to higher frequency (slow-3). Terms about visual function are associated with slow-3 and slow-5, further dividing the former type into two, the pathways of which ended in high and low frequency bands, respectively. These findings challenged the conventional binary segmentation of visual pathways (Schneider 1969) but provided fresh insights into the sophisticated visual perception mechanism (Freud et al. 2016). Notably, the ranking direction is opposite between the main part of the VN and the SMN/AN, indicating that visual and sensorimotor/auditory information processing and integration mechanisms may be different. This corresponds with previous findings that the power distribution pattern of the visual cortex is different from that of the precentral gyrus and the superior temporal gyrus (Gohel and Biswal 2015). The former exhibits more power at low frequencies and less power at high frequencies than the latter. Additionally, behavioral research has shown that the auditory process is superior to the visual process in working memory (Paivio et al. 1975; Goolkasian and Foos 2002; Pillai and Yathiraj 2017). Our findings indicate that the AN integrates information more quickly than the VN, which is consistent with behavioral observations. This suggests that investigating the brain-behavior association leveraging the multiband frequency analysis would provide more information to decode the brain mechanism.

The FPN and the DAN are also relatively homogenous in the frequency-rank map. These two networks are usually activated in cognitive control and attention-intensive tasks (Corbetta and Shulman 2002; Fox et al. 2005; Dosenbach et al. 2007). The highest integration level of the FPN is in slow-1 and slow-2, whereas the DAN is in slow-5 and slow-6, suggesting that the FPN can integrate information very fast, while the DAN integrates information in a more sustained process. The present results are in line with previous findings. The FPN is thought to provide control initiation and flexibility during information processing (Dosenbach et al. 2007), thus requiring fast processing capabilities. The DAN participates in the top-down processing of selecting external information as well as the maintenance of attention (Corbetta et al. 1998; Fox et al. 2006), both of which require ongoing processing over time. Furthermore, in the meta-analytic decoding results, attention is linked to slow-5. The VAN differentiates in the frequency-rank parcellation map. The ventral frontal cortex (VFC) displays the highest integration level in medium to high frequencies, whereas the temporal-parietal junction (TPJ) and the medial part of the VAN display the highest integration level in low frequencies. The VAN is involved in the bottom-up control of attention (Corbetta and Shulman 2002). Along with detecting salient stimuli, it also responds to task-relevant stimuli and interacts with the DAN (Corbetta and Shulman 2002). Consequently, the integration degree and speed requirements for the VAN may vary according to the type of stimuli and the degree of task involvement. This may help to explain why the VAN in the frequency-rank parcellation is heterogeneous.

The DMN is polarized into lateral and medial parts in the frequency-rank parcellation. The lateral part shows the highest integration level in slow-1, whereas the medial part shows the highest integration level in slow-6. According to a recent discovery, which examined the frequency-dependent FC characteristics among the DMN nodes, connections of the medial nodes are significantly reduced in high frequencies, whereas some of those of the lateral nodes are still present (Zhang et al. 2015). Additionally, a clinical study discovered frequency-dependent variations in the DMN between AD patients and healthy controls, demonstrating that the FC alterations are primarily in low frequencies (Li et al. 2017). The heterogeneity in the frequency domain suggests that the DMN operates differently and plays different roles at various frequencies. Additionally, our findings suggest that the DMN could be separated into medial and lateral subregions. On the axis of the first gradient, the DMN is considered to have the highest level of integration (Margulies et al. 2016). The two subregions of the DMN may be at the highest level of integration of two parallel sets of processing systems. Information that requires rapid processing speed or a continuous processing duration may be integrated by the lateral and medial DMN, respectively. Meta-analytic decoding results showed that self-related functions commonly thought to be associated with the DMN were integrated in slow-6. Future multiple frequency research should involve more in-depth studies to provide a deeper understanding of how the DMN and other networks function in both the spatial and frequency domains.

In sum, this study investigated the consistency and differences of FC gradient distribution across multiple frequency bands. Our results suggest that the coarse skeleton of the organizational hierarchy is generalizable across frequency bands. Align with previous gradient research, the unimodal-transmodal axis appeared as the first gradient in all six frequency bands and the visual-sensorimotor axis appeared as the second gradient in most frequency bands (Margulies et al. 2016). The omnipresence of the unimodal-transmodal axis across frequency bands as well as connectivity strength (Nenning et al. 2023) indicates its dominant role in the FC organization. Additionally, the large-scale brain networks are embodied by the frequency-rank map. The highest levels of integration, however, differ in the frequency domain across large-scale brain networks. These results show that information integration rates vary among brain networks. By combining frequency information with the unimodal-transmodal gradient, the direction of information flow would be emerged. Gradient analysis has been used to study cognition in several studies (Sormaz et al. 2018; Murphy et al. 2019). Our findings show the potential of leveraging the multi-band gradient method to decode cognition process.

Acknowledgments

CRediT author statement

Zhu-Qing Gong (Data curation, Formal analysis, Methodology, Resources, Software, Visualization, Writing—original draft, Writing—review & editing), Xi-Nian Zuo (Conceptualization, Formal analysis, Funding acquisition, Investigation, Methodology, Project administration, Supervision, Validation, Visualization, Writing—original draft, Writing—review & editing).

Funding

Conflict of interest statement: None declared.

Data availability

Data used in preparation of this article were obtained from the HCP (www.humanconnectome.org) and the CHCP database (www.Chinese-HCP.cn).

References

Aboitiz F. Brain connections: interhemispheric fiber systems and anatomical brain asymmetries in humans. *Biol Res*. 1992:25: 51–61.

Baria AT, Baliki MN, Parrish T, Apkarian AV. Anatomical and functional assemblies of brain BOLD oscillations. *J Neurosci*. 2011:31: 7910–7919.

Biswal B, Yetkin FZ, Haughton VM, Hyde JS. Functional connectivity in the motor cortex of resting human brain using echo-planar MRI. *Magn Reson Med*. 1995:34:537–541.

Buzsaki G, Draguhn A. Neuronal oscillations in cortical networks. *Science*. 2004:304:1926–1929.

Cabral J, Fernandes FF, Shemesh N. Intrinsic macroscale oscillatory modes driving long range functional connectivity in female rat brains detected by ultrafast fMRI. *Nat Commun*. 2023:14: 375–375.

Chen AC, Oathes DJ, Chang C, Bradley T, Zhou ZW, Williams LM, Glover GH, Deisseroth K, Etkin A. Causal interactions between fronto-parietal central executive and default-mode networks in humans. *Proc Natl Acad Sci USA*. 2013:110:19944–19949.

Corbetta M, Shulman GL. Control of goal-directed and stimulus-driven attention in the brain. *Nat Rev Neurosci*. 2002:3: 201–215.

Corbetta M, Akbudak E, Conturo TE, Snyder AZ, Ollinger JM, Drury HA, Linenweber MR, Petersen SE, Raichle ME, Van Essen DC, et al. A common network of functional areas for attention and eye movements. *Neuron*. 1998:21:761–773.

Dong H-M, Margulies DS, Zuo X-N, Holmes AJ. Shifting gradients of macroscale cortical organization mark the transition from childhood to adolescence. *Proc Natl Acad Sci USA*. 2021:118:e2024448118.

Dosenbach NUF, Fair DA, Miezin FM, Cohen AL, Wenger KK, Dosenbach RAT, Fox MD, Snyder AZ, Vincent JL, Raichle ME, et al. Distinct brain networks for adaptive and stable task control in humans. *Proc Natl Acad Sci USA*. 2007:104:11073–11078.

Engel AK, Fries P, Singer W. Dynamic predictions: oscillations and synchrony in top-down processing. *Nat Rev Neurosci*. 2001:2: 704–716.

Fox MD, Snyder AZ, Vincent JL, Corbetta M, Van Essen DC, Raichle ME. The human brain is intrinsically organized into dynamic, anti-correlated functional networks. *Proc Natl Acad Sci USA*. 2005:102: 9673–9678.

Fox MD, Corbetta M, Snyder AZ, Vincent JL, Raichle ME. Spontaneous neuronal activity distinguishes human dorsal and ventral attention systems. *Proc Natl Acad Sci USA*. 2006:103:10046–10051.

Freud E, Plaut DC, Behrmann M. 'What' is happening in the dorsal visual pathway. *Trends Cogn Sci*. 2016:20:773–784.

Frühholz S, Trost W, Grandjean D, Belin P. Neural oscillations in human auditory cortex revealed by fast fMRI during auditory perception. *NeuroImage*. 2020:207:116401.

Ge J, Yang G, Han M, Zhou S, Men W, Qin L, Lyu B, Li H, Wang H, Rao H, et al. Increasing diversity in connectomics with the Chinese Human Connectome Project. *Nat Neurosci*. 2023:26: 163–172.

Glasser MF, Sotiropoulos SN, Wilson JA, Coalson TS, Fischl B, Andersson JL, Xu J, Jbabdi S, Webster M, Polimeni JR, et al. The minimal preprocessing pipelines for the Human Connectome Project. *NeuroImage*. 2013:80:105–124.

Gohel SR, Biswal BB. Functional integration between brain regions at rest occurs in multiple-frequency bands. *Brain Connect*. 2015:5: 23–34.

Gong ZQ, Gao P, Jiang C, Xing XX, Zuo XN. DREAM: a toolbox to decode rhythms of the brain system. *Neuroinformatics*. 2021:19: 529–545.

Goolkasian P, Foos PW. Presentation format and its effect on working memory. *Mem Cogn*. 2002:30:1096–1105.

Hawrylycz MJ, Lein ES, Guillozet-Bongaarts AL, Shen EH, Ng L, Miller JA, van de lagemaat LN, Smith KA, Ebbert A, Riley ZL, et al. An anatomically comprehensive atlas of the adult human brain transcriptome. *Nature*. 2012:489:391–399.

Hong S-J, Xu T, Nikolaidis A, Smallwood J, Margulies DS, Bernhardt B, Vogelstein J, Milham MP. Toward a connectivity gradient-based framework for reproducible biomarker discovery. *NeuroImage*. 2020:223:117322.

Huntenburg JM, Bazin P-L, Goulas A, Tardif CL, Villringer A, Margulies DS. A systematic relationship between functional connectivity and intracortical myelin in the human cerebral cortex. *Cereb Cortex*. 2017:27:981–997.

Huntenburg JM, Bazin P-L, Margulies DS. Large-scale gradients in human cortical organization. *Trends Cogn Sci*. 2018:22:21–31.

Jamadar SD, Sforazzini F, Raniga P, Ferris NJ, Paton B, Bailey MJ, Brodtmann A, Yates PA, Donnan GA, Ward SA, et al. Sexual dimorphism of resting-state network connectivity in healthy ageing. *J Gerontol: Ser B*. 2018:74:1121–1131.

Kopell N, Ermentrout GB, Whittingtonm MA. Gamma rhythms and beta rhythms have different synchronization properties. *Proc Natl Acad Sci*. 2000:97:1867–1872.

Leech R, Scott G, Carhart-Harris R, Turkheimer F, Taylor-Robinson SD, Sharp DJ. Spatial dependencies between large-scale brain networks. *PLoS One*. 2014:9:e98500.

Li Y, Yao H, Lin P, Zheng L, Li C, Zhou B, Wang P, Zhang Z, Wang L, An N, et al. Frequency-dependent altered functional connections of default mode network in Alzheimer's disease. *Front Aging Neurosci*. 2017:9:259.

Li W, Wang M, Wen W, Huang Y, Chen X, Fan W, The Alzheimer's Disease Neuroimaging I. Neural dynamics during resting state: a functional magnetic resonance imaging exploration with reduction and visualization. *Complexity*. 2018:2018:4181649.

Li M, Gao Y, Ding Z, Gore JC. Power spectra reveal distinct BOLD resting-state time courses in white matter. *Proc Natl Acad Sci USA*. 2021:118:e2103104118.

Marek S, Tervo-Clemmens B, Calabro FJ, Montez DF, Kay BP, Hatoum AS, Donohue MR, Foran W, Miller RL, Hendrickson TJ, et al. Reproducible brain-wide association studies require thousands of individuals. *Nature*. 2022:603:654–660.

Margulies DS, Ghosh SS, Goulas A, Falkiewicz M, Huntenburg JM, Langs G, Bezgin G, Eickhoff SB, Castellanos FX, Petrides M, et al. Situating the default-mode network along a principal gradient of macroscale cortical organization. *Proc Natl Acad Sci USA*. 2016:113: 12574–12579.

Moran PAP. The interpretation of statistical maps. *J R Stat Soc Ser B Methodol*. 1948:10:243–251.

Murphy C, Wang H-T, Konu D, Lowndes R, Margulies DS, Jefferies E, Smallwood J. Modes of operation: a topographic neural gradient supporting stimulus dependent and independent cognition. *NeuroImage*. 2019:186:487–496.

Nenning K-H, Xu T, Franco AR, Swallow KM, Tambini A, Margulies DS, Smallwood J, Colcombe SJ, Milham MP. Omnipresence of the sensorimotor-association axis topography in the human connectome. *NeuroImage*. 2023:272:120059.

Noble S, Scheinost D, Constable RT. A decade of test-retest reliability of functional connectivity: a systematic review and meta-analysis. *NeuroImage*. 2019:203:116157.

O'Muncheartaigh J, Jbabdi S. Concurrent white matter bundles and grey matter networks using independent component analysis. *NeuroImage*. 2018:170:296–306.

Paivio A, Philipchalk R, Rowe EJ. Free and serial recall of pictures, sounds, and words. *Mem Cogn*. 1975:3:586–590.

Park Y-H, Cha J, Bourakova V, Lee J-M. Frequency specific contribution of intrinsic connectivity networks to the integration in brain networks. *Sci Rep*. 2019:9:4072.

Peer M, Nitzan M, Bick AS, Levin N, Arzyt S. Evidence for functional networks within the human brain's white matter. *J Neurosci*. 2017:37:6394–6407.

Penttonen M, Buzsáki G. Natural logarithmic relationship between brain oscillators. *Thalamus Relat Syst*. 2003:2:145–152.

Pillai R, Yathiraj A. Auditory, visual and auditory-visual memory and sequencing performance in typically developing children. *Int J Pediatr Otorhinolaryngol*. 2017:100:23–34.

Samara A, Eilbottb J, Margulies DS, Xud T, Vanderwal T. Cortical gradients during naturalistic processing are hierarchical and modality-specific. *NeuroImage*. 2023:271:120023.

Schneider GE. Two visual systems. *Science*. 1969:163:895–902.

Sormaz M, Murphy C, Wang H-т, Hymers M, Karapanagiotidis T, Poerio G, Margulies DS, Jefferies E, Smallwood J. Default mode network can support the level of detail in experience during active task states. *Proc Natl Acad Sci*. 2018:115:9318–9323.

Thompson WH, Fransson P. The frequency dimension of fMRI dynamic connectivity: network connectivity, functional hubs and integration in the resting brain. *NeuroImage*. 2015:121:227–242.

Van Essen DC, Smith SM, Barch DM, TEJ B, Yacoub E, Ugurbil K, WU-MH C. The WU-Minn Human Connectome Project: an overview. *NeuroImage*. 2013:80:62–79.

Wael R, Benkarim O, Paquola C, Lariviere S, Bernhardt BC. BrainSpace: a toolbox for the analysis of macroscale gradients in neuroimaging and connectomics datasets. *Commun Biol*. 2020:3:103.

Xue SW, Li D, Weng XC, Northoff G, Li DW. Different neural manifestations of two slow frequency bands in resting functional magnetic resonance imaging: a systemic survey at regional, interregional, and network levels. *Brain Connecti*. 2014:4: 242–255.

Yan L, Zhuo Y, Ye Y, Xie SX, An J, Aguirre GK, Wang J. Physiological origin of low-frequency drift in blood oxygen level dependent (BOLD) functional magnetic resonance imaging (fMRI). *Magn Reson Med*. 2009:61:819–827.

Yeo BTT, Krienen FM, Sepulcre J, Sabuncu MR, Lashkari D, Hollinshead M, Roffman JL, Smoller JW, Zoeller L, Polimeni JR, et al. The organization of the human cerebral cortex estimated by intrinsic functional connectivity. *J Neurophysiol*. 2011:106: 1125–1165.

Zhang X, Zang Z. Evaluate the efficacy and reliability of functional gradients in within-subject designs. *Hum Brain Mapp*. 2023:44: 2336–2344.

Zhang T, Xu P, Guo L, Chen R, Zhang R, He H, Xie Q, Liu T, Luo C, Yao D. Multivariate empirical mode decomposition based sub-frequency bands analysis of the default mode network: a resting-state fMRI data study. *Appl Informa*. 2015:2:2.

Zuo XN, Di Martino A, Kelly C, Shehzad ZE, Gee DG, Klein DF, Castellanos FX, Biswal BB, Milham MP. The oscillating brain: complex and reliable. *NeuroImage*. 2010:49:1432–1445.

Zuo XN, Xu T, Milham MP. Harnessing reliability for neuroscience research. *Nat Hum Behav*. 2019:3:768–771.